*Desalination and Water Treatment*
www.deswater.com

doi: 10.5004/dwt.2020.25336

184 (2020) 150–162
April

# Cr(VI) and phenol simultaneous removal using attapulgite-supported nanoscale zero-valent iron in the presence of persulfate

Hui Xu*, Shuhua Yang, Yajuan Zhang, Jing Tang, Lei Tian, Yong Chen*

*College of Petrochemical Technology, Lanzhou University of Technology, Lanzhou, China, Tel. +86 13639317927; emails: xuhui@lut.cn (H. Xu), chenylut@126.com (Y. Chen), yjk441389465@qq.com (S. Yang), 1799797925@qq.com (Y. Zhang), 122493279@qq.com (J. Tang), 2528989045@qq.com (L. Tian)*

Received 7 May 2019; Accepted 10 December 2019

**ABSTRACT**

In this paper, attapulgite (APT)-supported nanoscale zero-valent iron (nZVI) composites (nZVI/APT) were synthesized by chemical liquid phase reduction to remove Cr(VI) and phenol from aqueous solutions in the presence of persulfate (Ps). The structure of as-prepared nZVI/APT was characterized by various techniques. Various effects on the reduction of Cr(VI) and degradation of phenol were evaluated. Experimental results revealed that nZVI/APT composites at a relatively low Ps concentration can effectively remove Cr(VI) and phenol simultaneously, the removal efficiencies of Cr(VI) and phenol were 98.7% and 80.3% after 60 min, respectively. There was a good synergistic effect between nZVI/APT and persulfate for removal of Cr(VI) and phenol. APT as the supporter matrix could decrease the aggregation of nZVI and increase its reactivity. nZVI can not only act as a reductant for removal of Cr(VI) but also act as a catalyst to activate Ps and generate sulfate radicals for removal of phenol. The presence of persulfate has no obvious effect on the removal of Cr(VI), but has remarkably promoted phenol oxidation. This implies that the nZVI/APT nanocomposites can act as catalyst to activate persulfate for the simultaneous removal of heavy metal and organic pollutant for the actual wastewater treatment.

*Keywords:* Nanoscale zero-valent iron; Sulfate radical oxidation; Simultaneous removal; Cr(VI); Phenol

## 1. Introduction

Chromium is a typical water pollutant, mainly from the manufacturing and mining industry, electroplating plant chromium-containing wastewater. Hexavalent chromium (Cr(VI)) is nearly 100 times more toxic than Cr(III), and has been identified as a substance with serious carcinogenicity [1]. At present, the treatment of highly toxic Cr(VI) in water is mainly through various techniques such as adsorption [2], chemical reduction [3], electrolysis [4], photocatalysis [5]. Phenol and its derivatives are toxic aromatic compounds in the wastewater that are produced by petrochemical, textile, coating and pharmaceutical industry, which can cause serious environmental pollution and dramatically harm human health [6]. In fact, the co-existence of various organic compounds and heavy metal ions is a common phenomenon in wastewater, which greatly increases the risk to aquatic environment [7–9]. Therefore, it is significance of simultaneous removal of heavy metals and organic pollutants in the environmental remediation. A lot of methods have been developed and applied to remove complex pollutants in wastewater, including adsorption, chemical degradation and advanced oxidation processes (AOPs) [10]. Among the methods, adsorption is an efficient tool for phase transfer of contaminants [11,12]. That is the most common method used for removal of different types of pollutants from contaminated water because its low cost, simplicity of operator and high efficiency. Recently, nanoscale zero-valent iron (nZVI) has the advantages of large surface area, high reductive reactivity and environmental harmlessness, which makes it being widely

* Corresponding authors.

used for the removal of organic compounds and heavy metal ions [13]. However, high surface energy and intrinsic ferromagnetism of $Fe^0$ nanoparticles make them easy to aggregate and reduce their stability and chemical reactivity. In order to overcome these drawbacks, some researches have been focused on the combination of nZVI with different organic/inorganic support such as surfactants [14], clay minerals [15], graphene [16], activated carbon [17], etc. Clays have also been used as versatile matrices to embed or disperse metal nanoparticles for fabrication of composite nanomaterials, making composite both possess themselves properties and with playing a role of synergistic effect. The clay mineral attapulgite (APT), a form of magnesium aluminum silicate mineral, it has advantages of unique one-dimensional structures, high surface specific area and good cation exchange capacity compared with other clay minerals [18]. Attapulgite was widely used as low-cost adsorbent for removal of metal ions and organic pollutants. Nevertheless, APT exhibits poor performances such as long adsorption time, low adsorption efficiency and bad reusability. A feasible solution is to use as a stable substrate for loading nZVI and make APT with the abundant active sites to increase its adsorption efficiency. APT can be used as a support material for dispersion and stabilization of nZVI. The composite can be applied to environmental remediation treatment combined with excellent adsorption property and strong reducibility of nZVI, but less related researches on APT supported nZVI [19].

The AOP is considered to be the most effective way to remove toxic and degrading organic pollutants. Most AOPs generally use hydroxyl radical ($HO^{\bullet}$) ($E^0 = 2.8$ V) as the main oxidant to remove toxic and refractory contaminants [20]. However, its practical applications for industrial wastewater treatment have been limited by factors such as short life span (such as $H_2O_2$ or $O_3$ systems) and the Fenton reaction restricted pH [21,22]. In recent years, the application of AOPs based on activation of persulfate to generate the sulfate radicals ($SO_4^{\bullet-}$) with redox potential ($E^0 = 2.6$ V) has great potential for removing many refractory pollutants [23,24]. Persulfate can be activated by heat, ultraviolet radiation and transition metal ions to generate a stronger non-selective oxidant $SO_4^{\bullet-}$. In these activators, the $Fe^{2+}$ aqueous solution is the most suitable application for environmental treatment [24–26]. Similar to the traditional Fenton system ($Fe^{2+}$/$H_2O_2$), $Fe^{2+}$ is an efficient activator for the production of $SO_4^{\bullet-}$. However, the generation of sulfate radical anions by the reaction to dissolve $Fe^{2+}$ with persulfate is too fast to control, and excessive amounts of the generated iron needed further treatment. Lately, nZVI has been widely used in the Fenton-like reaction to remove organic contaminants. There are some researches about the activation of persulfate by nZVI to generate sulfate radical anions to remove organic compounds and heave metals in heterogeneous nZVI-Ps Fenton-like system [25,27]. nZVI could slow release of $Fe^{2+}$, which can activate persulfate, producing sulfate radical anions oxidation to removal of organic compounds. nZVI can not only be used as a reductant but also provide the alternative source of $Fe^{2+}$ and recycle $Fe^{3+}$ on its surface and reduce the precipitation of iron hydroxides during the reaction. The use of nZVI can overcome the shortcomings of $Fe^{2+}$, and avoid the introduction of other anions. Diao et al. [28] studied bentonite-supported nanoscale zero-valent iron/persulfate system for the simultaneous removal of Cr(VI) and phenol from aqueous solutions, but the removal rate of phenol was the lower. However, as far as we know, there are few studies about the effectiveness of the nZVI/APT-Ps Fenton-like process in the removal of Cr(VI) and phenol simultaneously in literature. Therefore, it appears significant to investigate the removal efficacy for specific pollutants of the novel composites.

In the study, the main object is to investigate the feasibility of nZVI/APT composite in the presence of persulfate for simultaneous removal of Cr(VI) and phenol in the simulated wastewater. The nZVI plays an important role in the removal of pollutants by measuring the Fe content in the solution. nZVI not only can be used as a reductant for removal of Cr(VI) but also act as a catalyst to activate Ps and generate sulfate radicals for removal of phenol. The removal of phenol was mainly attributed to that nZVI can react with Cr(VI) to produce $Fe^{2+}$ in acidic conditions, and dissolved $Fe^{2+}$ can activate persulfate to produce sulfate radical anions to oxidize phenol for removal. The presence of persulfate has no obvious effect on the removal of Cr(VI), but has remarkably promoted phenol oxidation. There was a good synergistic effect between nZVI/APT and persulfate for removal of Cr(VI) and phenol. The environment-friendly APT clay as the supporter matrix could effectively decrease the aggregation of nZVI and increase its reactivity. For the application in the environment and industry, the nZVI/APT combined Ps system provides a cost-effective and environmentally green method for simultaneous removal of Cr(VI) and phenol. Meanwhile, the different single factor experiments on the reduction of Cr(VI) and degradation of phenol were evaluated. The effect of persulfate in the system was elucidated and the proposed degradation pathways of Cr(VI) and of phenol were also analyzed. In addition, the experimental parameters of adsorption thermodynamics and kinetic models provided the basis for the adsorption mechanism analysis, indicating that the degradation process on Cr(VI) and phenol by nZVI/APT belongs to single molecular layer chemical adsorption.

## 2. Experimental

### 2.1. Materials

Attapulgite (99%, APT; JC-J503) was purchased from Jiangsu Xuyi Nano-materials Science and Technology Co. Ltd., China. Potassium dichromate ($K_2Cr_2O_7$) was purchased from Tianjin Tianxin chemical factory, Chemical Reagents Co. Ltd., China. Ferrous sulfate ($FeSO_4{\cdot}7H_2O$) was purchased from Tianjin Kaixin Chemical Reagent Co. Ltd., China. Potassium persulfate ($K_2S_2O_8$) was purchased from Shanghai Zhongqin chemical reagents Co. Ltd., China. Sodium borohydride ($NaBH_4$) was purchased Sinopharm Chemical Reagent Co. Ltd., China. All chemicals were of analytical grade and all solutions were prepared with distilled water.

### 2.2. Preparation of nZVI/APT

nZVI/APT was prepared using a conventional liquid-phase method via the reduction of ferric iron by borohydride with attapulgite as a support material. In a typical procedure, 4.978 g of $FeSO_4{\cdot}7H_2O$ was added into a 250 mL

flask, and then stirred by adding 50 mL distilled water to dissolve. Then, 1 g of attapulgite was added to the above solution for mixing, and ultra-sonication was carried out for 20 min. Under the $N_2$ protection, the newly prepared solution of $NaBH_4$ (2.0312 g dissolved in 100 mL distilled water) was added drop-wise into the stirred mixture. After the drip was completed, the solution was stirred continuously for another 20 min and then by vacuum filtration, with anhydrous ethanol washed three times. The solid was then dried at 60°C under vacuum overnight. The nZVI was prepared under identical conditions but without attapulgite.

### 2.3. Characterization of the nZVI/APT

Morphology and structure of composite materials were observed by transmission electron microscope (TEM, JEM-1200EX, United States). Fourier transforms infrared concerning composite materials was obtained employing Fourier transform infrared spectroscope (FT-IR, NEXQS670, United States) using KBr pellets. X-ray diffraction patterns were collected on an X-ray powder diffractometer (XRD, D/MAX–2400X, Japan) with Cu-K$\alpha$ radiation ($\lambda$ = 0.15406 Å) in a 2$\theta$ range of 5°–80° at room temperature. The specific surface area (SSA) of nZVI and nZVI/APT were tested using the BET-$N_2$ adsorption method (BET, ASAP 2020, United States). The pH measurements were conducted with a glass electrode (PHS-3D Model pH meter, China). The Cr(VI) and phenol concentrations were determined with a UV–Vis spectrophotometer (UV-1900, Shanghai).

### 2.4. Experimental procedures and analytical methods

The dosage of nZVI/APT was 1 g/L, and the initial pH was kept at 3 (pH was adjusted by 0.1 M HCl and 0.5 M NaOH solutions) in the reaction. Batch experiments were conducted in concentration of persulfate, Cr(VI) and phenol were 2 mM, 30 and 20 mg/L, respectively. For all adsorption runs, 50 mL solution containing certain amount Cr(VI) and phenol at 298 K.

The concentration of Cr(VI) was determined by the 1,5-diphenylcarbazide colorimetric method monitoring the absorbance at 540 nm in acidic solution with a UV-Vis spectrophotometer. The steps of the determination method were as follows: 1 mL samples, then added 0.5 mL sulfuric acid phosphoric acid solution and 2 mL 1,5-diphenylcarbazide ternary solution were mixed together. The absorbance of the solutions was measured at 540 nm for the generated purple colored complex compound after full color development.

The concentration of phenol was determined by the 4-aminoantipyrine method monitoring the absorbance at 510 nm with a UV-Vis spectrophotometer. Before the analysis, phenol was converted into a complex by adding 0.5 mL buffer solution (ammonia + ammonium chloride) adjusted pH about 10 and 1 mL 0.05 mol/L 4-aminoantipyrene and 1 mL of 0.05 mol/L potassium ferricyanide, then the solution will be obtained the brown-red dye and measured the absorbance at 510 nm with a UV-Vis spectrophotometer.

In this study, the persulfate solution 1–6 mM was prepared, compared with the removal efficiency of phenol and Cr(VI) when presence or absence of persulfate and different concentrations.

The adsorption capacity and removal efficiency of Cr(VI) were calculated using Eqs. (1) and (2), and phenol by Eqs. (3) and (4):

$$q_e = \frac{C_0 - C_t}{m} \times V \tag{1}$$

$$R = \frac{C_0 - C_t}{C_0} \times 100\% \tag{2}$$

$$q_e = \frac{C_0 - C_t \times 1{,}000}{m} \times V \tag{3}$$

$$R = \frac{C_0 - C_t \times 1{,}000}{C_0} \times 100\% \tag{4}$$

where $R$ (%) and $q_e$ are the removal efficiency and adsorption capacity of Cr(VI) and phenol, respectively; $C_0$ and $C_e$ are the initial and $t$ min concentrations of Cr(VI) and phenol in solution (mg/L).

To investigate the effect of free radicals in the removal of Cr(VI) and phenol, tert-butanol and ethanol were used as scavengers for sulfate radicals and hydroxyl radicals, respectively. Tert-butanol and ethanol were with molar ratios 1:1 (the quantity of tert-butanol and ethanol, respectively, was added 1 mL and 1 mol/L) at different reaction times of scavenger to phenol or Cr(VI) in this study. Aliquots of suspension were collected centrifuged for later analysis.

## 3. Results and discussion

### 3.1. Characterization of catalyst

The XRD patterns of nZVI and nZVI/APT are shown in Fig. 1. The nZVI showed a weak and broad peak at about 2$\theta$ = 44.6°, which were indexed to the (110) planes and consistent with the standard XRD corresponding to the body-centered cubic iron(0) (JCPDS card no. 06-0696) [29]. The presence of iron oxide with weak intensities in the XRD

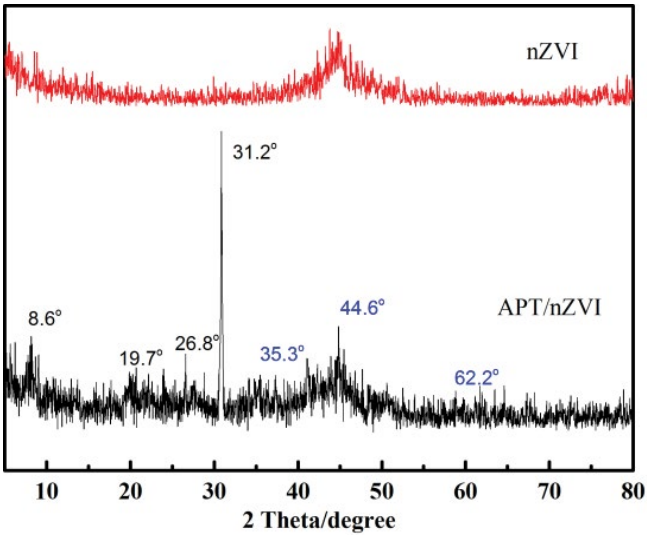


Fig. 1. XRD patterns of nZVI and nZVI/APT.

pattern of the nZVI particles (2θ = 35.3°, 62.2°) [30], which due to the surface of nZVI was oxidized. It can be seen that a characteristic peaks at 2θ = 8.6°, 19.7°, 26.8° consistent with the standard peak of APT [31], indicated that the structure of APT was maintained very well in the preparation process. The high intensity diffraction peak at 2θ = 31.2° which attributed to quartz. The XRD patterns of nZVI/APT composites showed an obvious characteristic diffraction peak of nZVI appearing at 2θ = 44.6°, indicating that the nano zero-valent iron has been successfully supported on APT.

Fig. 2 shows the XPS curve of prepared nZVI/APT. It demonstrates adsorbant nZVI/APT surface mainly contained Fe, O, C and Cr(VI) elements, at the same time amount of N and S (Fig. 2a). The curve of Fig. 2b was adsorbant before reaction with pollutants, the peaks at 706.8 and 720.0 eV belonged to $Fe^0$, indicating that the composites nZVI/APT were successfully prepared. In addition, the peaks at 710.5, 712.2 and 724.5 eV were assigned to Fe(II)/Fe(III) (Fe 2p3/2), Fe(III) (Fe 2p3/2) and Fe(III) (Fe 2p1/2), respectively [32,33]. As can be seen, the peaks of Fe(III) and Fe(II) existing in the sample confirmed that parts of nZVI were oxidized and formed a thin oxidation layer on the adsorbents' surface before reaction. After reaction, the peak at 706.8 eV was disappeared and the peak at 720.0 eV was significantly weakened. Meanwhile, the percentage of iron decreased from 23.62% before the reaction to 8.93%, which all declare that nZVI played an important part in the reaction process. The result was corresponding to the analysis of XRD. The new peaks around 575–590 eV corresponded to Cr2p in Fig. 2d [34]. As can be seen, the peaks at 579.5 and 589.3 eV were attributed to the Cr(VI) 2p, while the peaks at 575.6 and 585.2 eV belong to the Cr(III) 2p [35]. And after reaction, the total peaks intensity of Cr(VI) was 18%, however the Cr(III) was 82%. All the results indicated that Cr(VI) was adsorbed on the surface of nZVI/APT and reduced to Cr(III) by nZVI. Finally, it was removed by reacting with $Fe^{2+}$ to form $FeCr_2O_4$ [35].

The surface morphology images of the nZVI and nZVI/APT composite were evaluated by TEM. As shown in Fig. 3a, it has been seen that spherical nZVI particles seriously aggregate and form prominent chain-like aggregates because of their magnetic property, the ground magnetic force, and the magnetic force between the particles and the surface tension. The nZVI granules in Fig. 3b were obviously dispersed, the nZVI spherical granular loaded on the surface of rod-like APT and have diameters within 100 nm. The results demonstrated that APT as a support material was effective in reducing the aggregation and accelerating the dispersion of nZVI. After reaction with phenol and Cr(VI) in Fig. 3c, where obviously observed the number of nZVI was greatly decreased, implying nZVI plays a major role in the reaction process and APT supported nZVI could greatly improve the reactivity of nZVI particles.

The $N_2$ adsorption–desorption isotherms and pore size distributions of nZVI/APT were shown in Fig. 4. The BET parameters of the nZVI and nZVI/APT composite are shown in Table 1, and indicated that the composite nZVI/APT mainly contains mesoporosity. The BET SSAs of nZVI/APT and nZVI

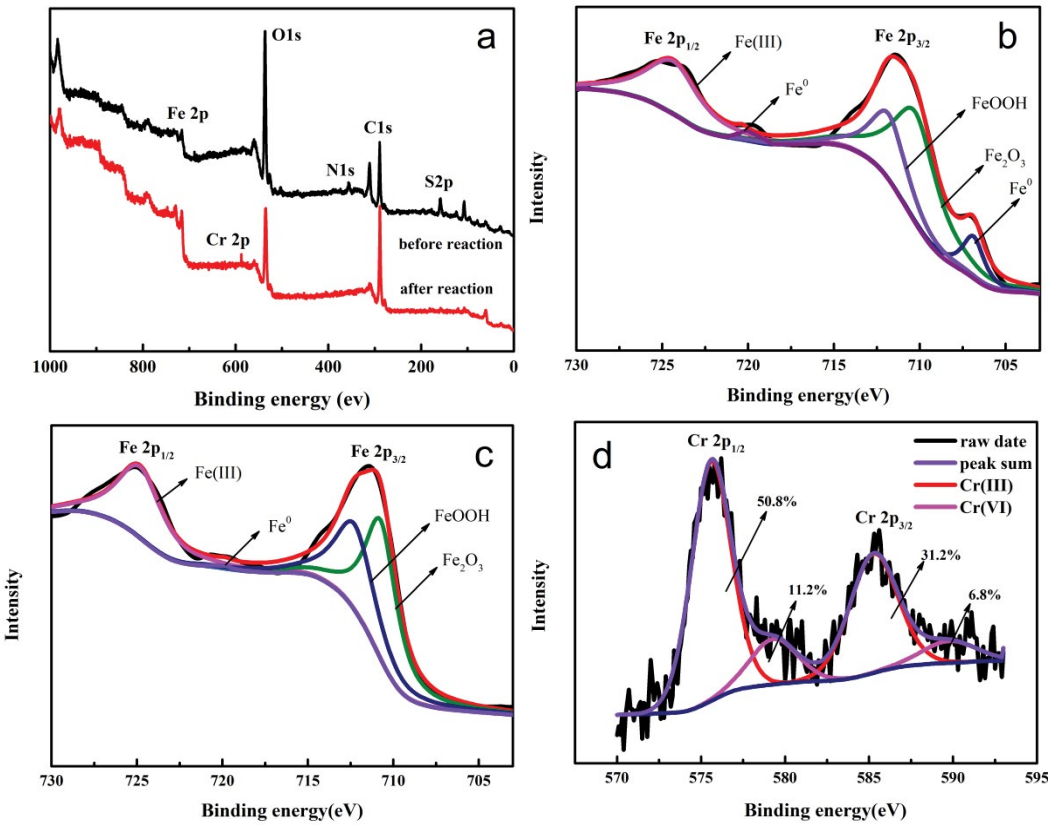


Fig. 2. XPS spectra of nZVI/APT: (a) full spectra; (b) and (c) Fe 2p of reaction before and after, (d) Cr 2p after reaction.

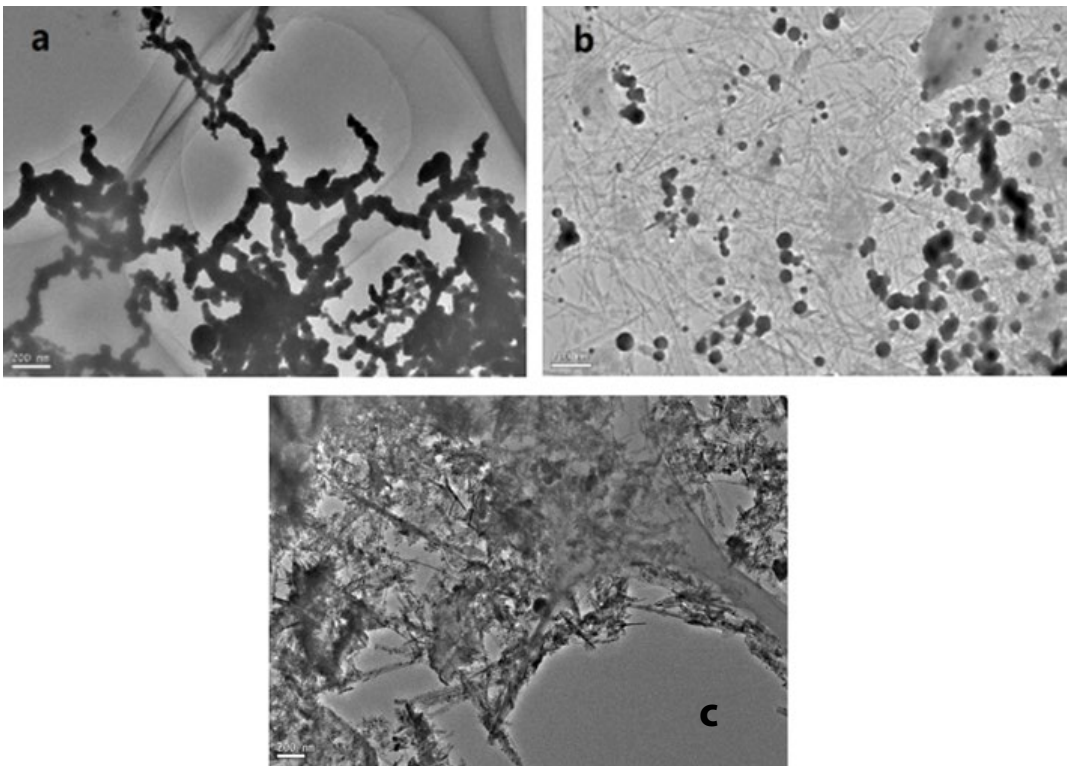


Fig. 3. TEM images of nZVI (a), nZVI/APT (b) and nZVI/APT after reaction with pollutions (c).

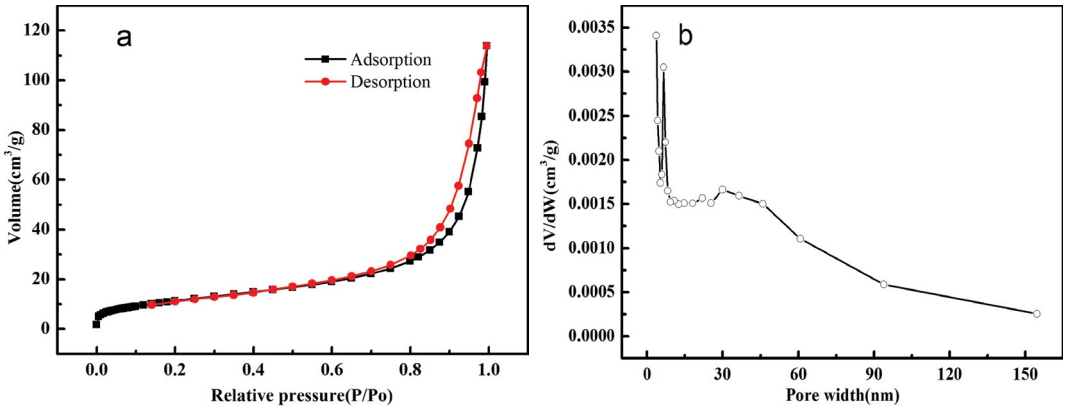


Fig. 4. $N_2$ adsorption–desorption isotherm (a) and pore size distribution (b) of nZVI/APT.

Table 1
BET parameters of nZVI and nZVI/APT

| | nZVI | nZVI/APT |
|---|---|---|
| BET surface area ($m^2/g$) | 17.51 | 54.20 |
| Total pore volume ($cm^3/g$) | 0.0455 | 0.1323 |
| Adsorption average pore width(4V/A by BET) (nm) | 103.9 | 97.61 |

were 54.2 and 17.5 $m^2/g$, respectively. The results show that the SSA of the nZVI/APT composite was nearly three times that of nZVI, which mainly due to the porous structure of APT and improvement of the dispersion of nZVI.

The FT-IR spectrum of APT, nZVI/APT composite and nZVI/APT after reaction with pollutants are revealed in Fig. 5. The strong absorption peaks at 3,553 and 3,416 $cm^{-1}$ belong to the –OH group in the attapulgite, which are the stretching vibration peaks of Al–OH and the stretching vibration peak of Mg–OH [36]; The characteristic absorption peak at 1,651 $cm^{-1}$ is the stretching vibration of zeolite water. The characteristic peaks appearing at 1,027 and 985 $cm^{-1}$ correspond to the skeleton structure of attapulgite [37], where the Si–O–Si peak at 1,027 $cm^{-1}$ and the Si–OH peak at 985 $cm^{-1}$ demonstrate the presence of nanorod-like structures of attapulgite; The absorption peak at 468 $cm^{-1}$ is attributed to the stretching vibration of $\delta_{Si-O}$ [31]. Compared with the reaction before, the peaks of reaction after is no obvious change, so

we applied other tests to characterize the surface elements changes in the material after the reaction. Consider the wavenumbers of the main characteristic peaks of APT, it means the supported nZVI has no change in the skeleton of APT.

### 3.2. Parameters affecting degradation of Cr(VI) and phenol

#### 3.2.1. Removal of Cr(VI) and phenol by different materials

At 298 K, the concentration of persulfate was 2 mM, and 50 mg of different materials APT, nZVI and nZVI/APT were used to remove 50 mL of Cr(VI) and phenol aqueous solution (adjusted solution pH = 3) with initial concentrations of 30 and 20 mg/L, respectively. The effect of different materials APT, nZVI and nZVI/APT on removal Cr(VI) and phenol in the presence of Ps is shown in Fig. 6. As presented in Fig. 6a, the results indicated that nZVI/APT was proved to be the most efficient in that more than 98.7% of Cr(VI) was removed after 60 min, while approximately 83.1% of Cr(VI) was removed using nZVI and a mere 6.3% for APT. The efficiency of removing Cr(VI) in aqueous solution using nZVI/APT was higher than nZVI since APT as a support material could disperse and stabilize nZVI as well as increase the reactivity and decrease the aggregation of the nZVI. APT has the lowest removal rate of Cr(VI), and it was only the adsorption effect of APT. For the removal of phenol as shown in Fig. 6b, the removal efficiency of phenol by nZVI/APT was 80.3% after 60 min, whereas about 36.4% and 9.7% of phenol was removed with nZVI and APT, respectively. It was observed that removal efficiency of phenol by nZVI/APT was highest, suggesting that nZVI/APT in the presence of Ps exhibited a high reactivity toward phenol oxidation. The removal of phenol was mainly in the acidic conditions nZVI/APT can produce $Fe^{2+}$ and electrons [25], as well as nZVI reacts with Cr(VI), $Fe^{2+}$ can activate persulfate to produce sulfate radical anions. Sulfate radical anions can oxidize phenol and then achieve the purpose of removal [38]. The simultaneous removal efficiencies of Cr(VI) and phenol by nZVI/APT in the presence of Ps were 98.7% and 80.3% after 60 min, respectively. The result revealed that the simultaneous removal of Cr(VI) and phenol could be achieved by nZVI/APT composites in the presence of Ps.

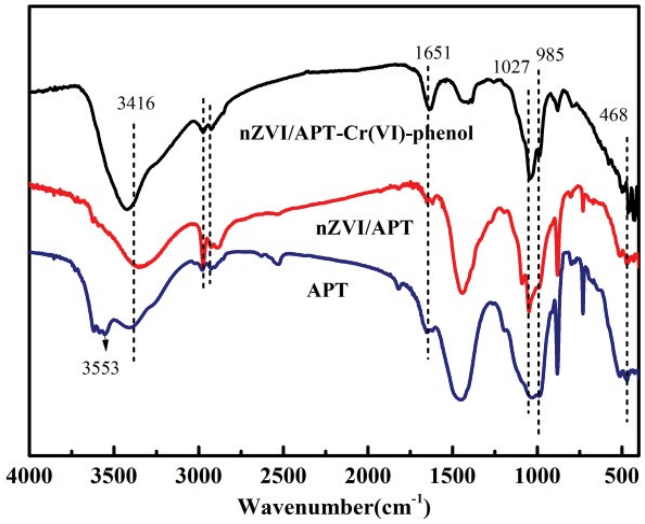


Fig. 5. FTIR images of APT and nZVI/APT and nZVI/APT after reaction with pollutants.

Table 2 shows the comparison of Cr(VI) and phenol co-removal by different materials under different experimental conditions. It can be seen that nZVI/APT in the presence of Ps is more efficient for removal of Cr(VI) and phenol than the other adsorbents.

#### 3.2.2. Effect of nZVI and APT ratios

To evaluate the reactivity of nZVI in the removal process of Cr(VI) and phenol in aqueous solution, effect of different nZVI and APT mass ratios on the removal efficiency of Cr(VI) and phenol in the presence of Ps was investigated. As shown in Fig. 7a, the removal of Cr(VI) increased with the increase of the attapulgite/iron mass ratio from 1:1 to 2:1, but further increasing the amount of nZVI (attapulgite/iron mass ratio:1:2 to 1:1) did not enhance the Cr(VI) removal performance notably. Although both removal efficiencies and reaction rates of Cr(VI) for nZVI/ATP (1:1) were lower than the other two mass ratio composites in the first 30 min. The removal of Cr(VI) by three different mass ratio were all nearly above 99% after 120 min, which indicated that APT can prevent the agglomeration of nZVI and enhance the reactivity of nZVI

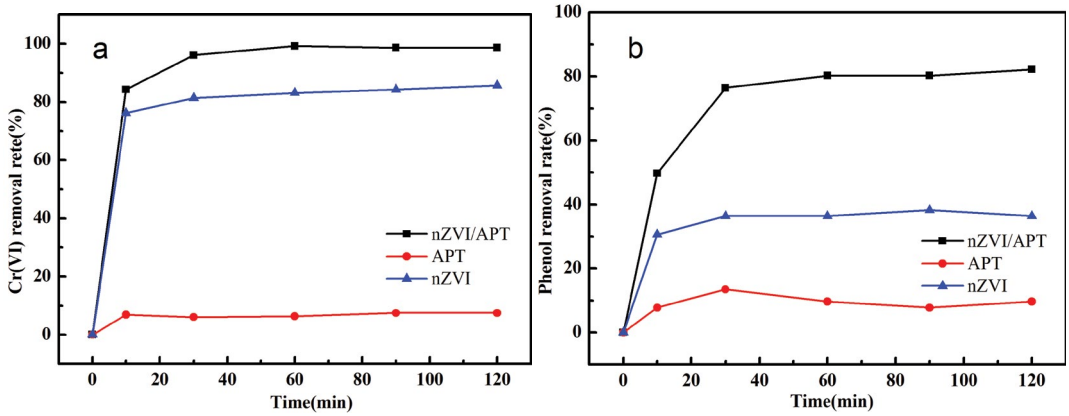


Fig. 6. Removal of Cr(VI) (a) and phenol (b) by nZVI, APT and nZVI/APT.

Table 2
Comparison of removal rate of various systems for Cr(VI) and phenol

| | Initial concentration | | | | | Removal rate (%) | | |
|---|---|---|---|---|---|---|---|---|
| Materials | Cr (VI) | Phenol | *T* (°C) | Time | pH | Cr(VI) | Phenol | References |
| *Acinetobacter guillouiae* SFC 500-1A | 10 mg/L | 300 mg/L | 28°C ± 2°C | 7 h | 4–7 | 38 (±3.9) | 54.2 (±1.2) | [39] |
| B/nZVI/Ps | 0.38 mM | 0.11 mM | 25°C ± 1°C | 30 min | 5 | 99.3 | 71.5 | [28] |
| $WS_2$-cocatalytic | 40 mg/L | 10 mg/L | – | 5 min | 3.5–4 | 80 | 60 | [40] |
| BiOI/rGO/$Bi_2S_3$ | 50 mg/L | 10 mg/L | – | 4 h | 3 | 73 | 95 | [41] |
| CFR | – | 100 mg/L | 30°C | 60 min | 2–8 | – | 93 | [42] |
| AC-peanut shell | 30 mg/L | – | 25°C | 24 h | 2–4 | 46.6 | – | [43] |
| $H_3PO_4$-peanut shell | 80 mg/L | – | 25°C | 240 min | 2 | 96.0 | – | [44] |
| nZVI/APT-Ps | 30 mg/L | 20 mg/L | 25°C ± 2°C | 60 min | 3 | 98.7 | 80.3 | This work |

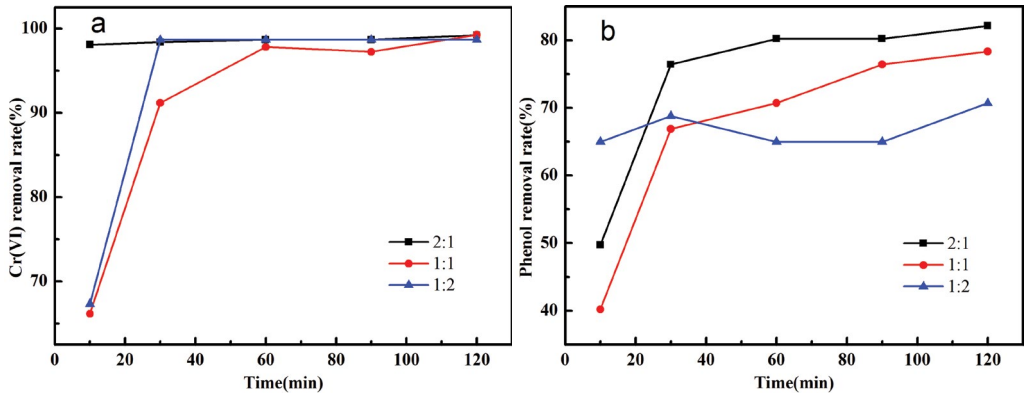


Fig. 7. Effect of different $m_{APT}$:$mn_{ZVI}$ mass ratio on degradation of Cr(VI) (a) and phenol (b).

in the composite. From Fig. 7b, it can be seen that when the APT/nZVI mass ratios were 2:1, 1:1 and 1:2, the removal efficiencies of phenol at 120 min were 82.2%, 78.3% and 70.7%, respectively. In the acidic conditions (pH = 3), nZVI/APT can easily produce $Fe^{2+}$ and it could activate persulfate to generate sulfate radical anions, and then phenol was removed by oxidization. Taking into account the removal efficiencies and reaction rates of Cr(VI) and phenol, the ratio of 2:1 was adopted as the optimal mass ratio for the following experiments finally.

### 3.2.3. Effect of pH value

The pH value of solution is the main factor affecting the degradation of Cr(VI) and phenol, and its function is to control the catalytic activity. Fig. 8a depicts the profiles of Cr(VI) and phenol removal efficiencies at different pH values when the reaction time was 60 min. As shown in Fig. 8a, when the pH varies from 3 to 10, the removal efficiencies of Cr(VI) were above 98% in this range. It can be seen that pH has almost no effect on the removal of Cr(VI), which revealed that the nZVI/APT composite has high reactivity with Cr(VI) and can effectively remove Cr(VI). However, the removal efficiency is slightly lower at pH = 10, it is attributed to the fact that $Fe^{3+}$ and $Fe^{2+}$ could form iron hydroxide on the surface of nZVI/APT to hinder the removal of Cr(VI). The influence of APT and nZVI/APT at different pH values on their surface electrical properties was studied using zeta potential in Fig. 8b. It can be seen that the isoelectric point (pH of zero point charge, $pH_{pzc}$) of APT and nZVI/APT was 2.5 and 4.9, respectively. At pH > $pH_{pzc}$, APT and nZVI/APT surfaces have net negative charge, while at pH < $pH_{pzc}$, surface have positive charge [30]. In the experiment, when pH < 4.9, the surface of nZVI/APT was positive charge, which will be conducive for the electrostatic attraction of $Cr_2O_7^{2-}$ and $CrO_4^{2-}$ and accelerate the reduction and degradation of Cr(VI) by nZVI, as well as the production of $Fe^{2+}$.

The results indicated that phenol removal efficiency decreased with the increase of pH value in Fig. 8a. When the pH values of the mixed solution were 3, 5, 7 and 10, the removal efficiencies of phenol by nZVI/APT-Ps after 60 min were 80.3%, 55.4%, 51.6% and 38.3%, respectively. The results show that phenol has high removal efficiency under acidic conditions. This is due to the more dissolved $Fe^{2+}$ and electrons production under acidic conditions [45]. Dissolved $Fe^{2+}$ could activate persulfate to generate more sulfate radical anions to oxidize phenol. Furthermore, under neutral and alkaline conditions, $Fe^{3+}$ and $Fe^{2+}$ could form iron hydroxide

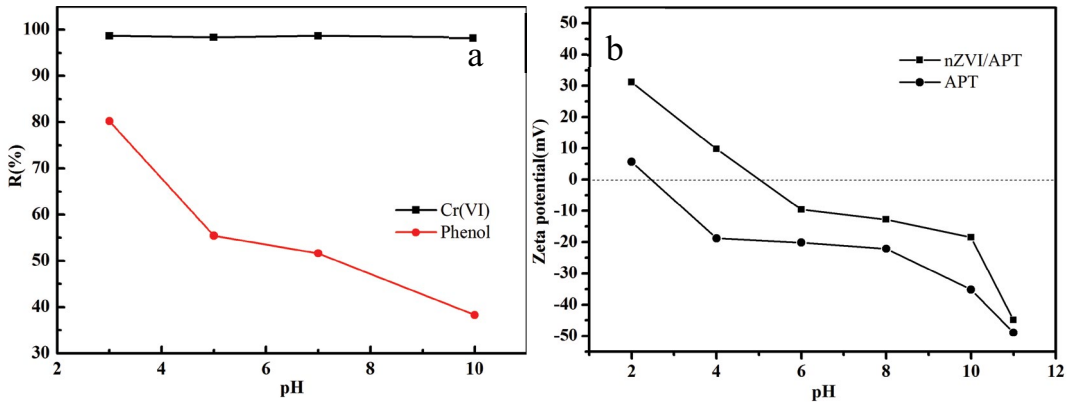


Fig. 8. Effect of pH value on the Cr(VI) and phenol removal (a); Zeta potential of APT and nZVI/APT (b).

on the surface of nZVI/APT, hindering the generation and release of $Fe^{2+}$ [38].

### 3.2.4. Effect of Ps

Effect of Ps on the removal of Cr(VI) and phenol is presented in Fig. 9a. As shown in Fig. 9a, it was observed that the removal rate of phenol increased from 31.1% to 86.2% after 120 min when persulfate was added. The enhanced removal of phenol was mainly attributed to catalytic persulfate oxidation. Compared with the nZVI/APT without persulfate, the removal rate of Cr(VI) increased from 97.8% and 99.2%, indicating that the presence of persulfate could not reduce nZVI reactivity toward Cr(VI) but remarkably promote phenol oxidation. The results clearly demonstrated that the simultaneous removal of Cr(VI) and phenol could be successfully achieved by nZVI/APT in the presence of Ps. Moreover, there is no obvious difference in Cr(VI) removal when the Ps concentration in the range of 1–6 mM (Fig. 9b), which further indicated that the presence of Ps had no negative effect on the removal of Cr(VI). It is mainly due to the existing excess nZVI, meaning that reduction activity of nZVI is sufficient to remove Cr(VI). The formed Cr(III) species would not be reoxidized into Cr(VI) in the presence of persulfate and sulfate radical anions. When the concentration of Ps was 2 mM, the removal efficiency of phenol was 82.2% after 120 min. It was found that the removal efficiency of phenol decreased gradually when the concentration of Ps exceeded 2 mM, which may be due to the sulfate radical anions self-scavenging. In addition, the $Fe^{2+}$ can react with sulfate radical anions, which consumes part of the sulfate radical anions, leading to the decrease of removal rate of phenol [45,46].

### 3.2.5. Effect of Cr(VI)/phenol concentration ratios

Fig. 9c shows that the Cr(VI) removal efficiency is above 98% after 60 min, and there is almost no significant difference within the Cr(VI)/phenol concentration ratio range of 3:1–3:6. However, the removal efficiency of phenol gradually decreases with the increase of phenol concentration. When Cr(VI)/phenol concentration ratios were 3:1, 3:2, 3:3 and 3:6, the removal efficiencies of phenol at 60 min were 83.4%, 80.3%, 48.7% and 18.4%, respectively. It could be interpreted that the removal efficiency of phenol was decreased, a large number of $SO_4^{\bullet-}$ radicals were consumed with the increase of phenol concentration, it hindered the removal of phenol. Furthermore, the Cr(VI) concentration didn't change that lead to produce number of $Fe^{2+}$ keep constant, and meanwhile $Fe^{2+}$ activation persulfate produces a certain amount of $SO_4^{\bullet-}$ radicals [46] resulting in phenol removal performance decreased.

### 3.2.6. Fe content in the solution after removal of pollutants and the regeneration of adsorbent

Single-factor experimental analysis showed that nZVI played an important role in removing phenol and Cr(VI), and the dissolved content of Fe in the solution was also the focus in this study, and the research results are shown in Fig. 10a. The concentration of total Fe and $Fe^{3+}$ was increased with reaction, due to a redox reaction between iron and chromium and iron is oxidized to $Fe^{2+}$ and $Fe^{3+}$. However, the content of $Fe^{2+}$ remained below 1.5 mg/L that mainly because it was used to activate persulfate to generate $SO_4^{\bullet-}$ and oxidize phenol.

The regeneration of nZVI/APT was carried out with 20 mg/L phenol and 30 mg/L Cr(VI) solution and 0.5 g adsorbent dosage at pH was 3. After reacting with phenol and Cr(VI) for 60 min, the adsorbents were desorbed by distilled water. The result is shown in Fig. 10a. Removal efficiency of the nZVI/APT gradually declined with number of cycles increase. At the first cycle, the removal efficiency was 95% and 84.5% for phenol and Cr(VI), but after fifth cycle the removal rate was only 49.7% and 12.5%, respectively. The main reason was that the consumption of nZVI and Ps increased and there were no excess active sites for adsorption of pollutants with the increase of the cycle of reuse.

## 3.3. Kinetic study of nZVI/APT

Adsorption capacity is one of the important parameters for adsorbents. And adsorption kinetics is an important tool to study the adsorption process and control the adsorption rate to obtain relevant kinetic parameters [47]. As can be seen from Fig. 11, the adsorption and degradation was fast in the first 40 min and the reaction adsorption equilibrium was reached at 200 min. With the increase of concentration, the adsorption capacity of nZVI/APT on Cr(VI) augments rapidly

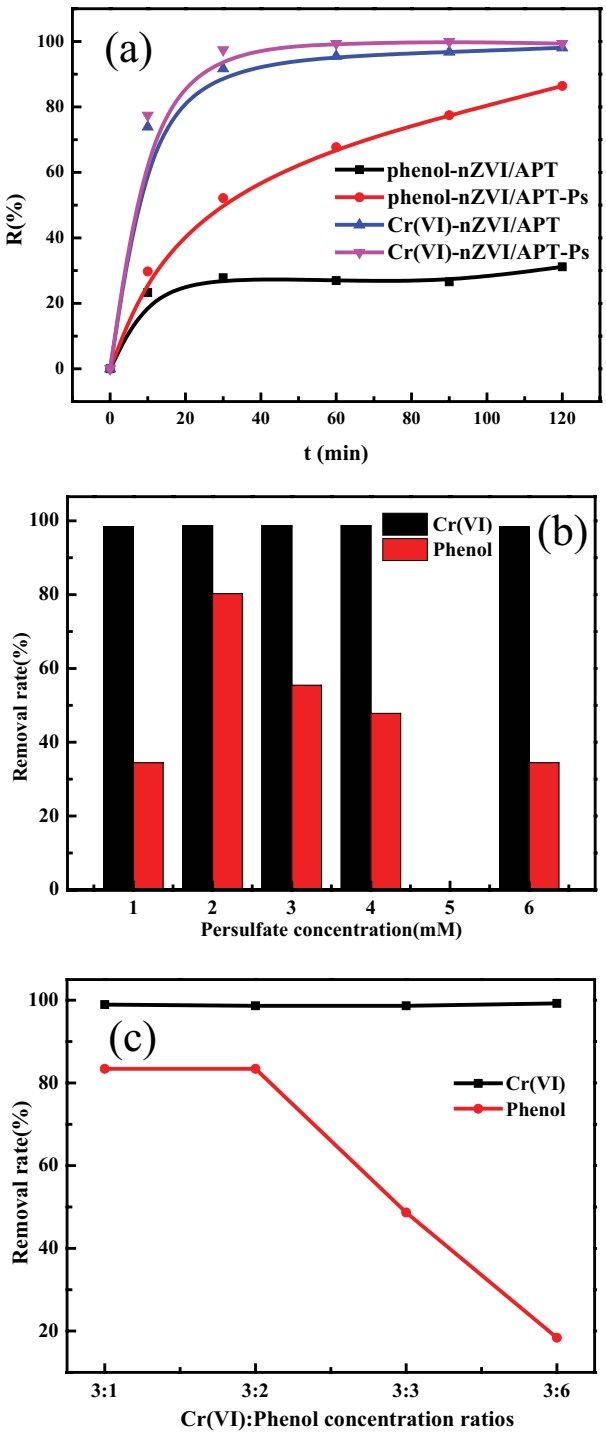


Fig. 9. Simultaneous removal of Cr(VI) and phenol by nZVI/APT, nZVI/APT-Ps system (a); effect of Ps concentration on removal of Cr(VI) and phenol (b); effect of Cr(VI)/phenol concentration ratios on removal of Cr(VI) and phenol (c).

than phenol. It can be seen that nZVI plays an important role in degradation of pollutants at composite materials.

In order to study the control mechanism of adsorption process, different kinetic models are applied such as pseudo-first order (PFO), pseudo-second order (PSO) and intra-particle diffusion (ID). The forms of the equations are, respectively, expressed by using Eqs. (5)–(7):

$$\ln(q_e - q_t) = \ln q_e - K_1 t \tag{5}$$

$$\frac{t}{q_t} = \frac{t}{k_2 q_e^2} + \frac{t}{q_e} \tag{6}$$

$$q_t = k_p \sqrt{t} + C \tag{7}$$

where $k_1$ (min$^{-1}$) is the rate constant of pseudo-first order model adsorption, $k_2$ (g·(mg min)$^{-1}$) is the rate constant of pseudo-second order model adsorption, $q_e$ (mg/g) is the adsorption capacity at equilibrium, $q_t$ (mg/g) is the adsorption capacity at time $t$, $t$ (min) is contact time, $k_p$ (mg·(g min$^{1/2}$)$^{-1}$) is the rate constant of intra-particle diffusion kinetic models and $C$ is constant. The values of kinetic parameters are listed in Table 3.

From the analysis of Table 3, the correlation coefficient of the pseudo-second order kinetic model is closer to 1. This suggests that the pseudo-second order can better describe the nZVI/APT remove of phenol and Cr(VI). Because the pseudo-second order kinetic model is based on the assumption that the adsorption rate is controlled by the chemical adsorption mechanism, the rate of the adsorption process is controlled by the chemical adsorption process.

### 3.4. Adsorption isotherms study of nZVI/APT

Adsorption isotherm is an effective method to study the interaction between adsorbent and adsorbant [48]. In this study, the following Langmuir (Eq. (8)), Freundlich (Eq. (9)) and Temkin (Eq. (10)) models to be used:

$$\frac{C_e}{q_e} = \frac{C_e}{q_m} + \frac{1}{q_m b} \tag{8}$$

$$\ln q_e = \ln K_F + \frac{1}{n} \ln C_e \tag{9}$$

$$q_e = \beta \ln K_T + \beta \ln C_e \tag{10}$$

where $q_m$ (mg/g) is the calculated adsorption capacity at maximum, $q_e$ (mg/g) is the experimental adsorption capacity at equilibrium, $C_e$ (mg/L) is the equilibrium concentration of the solution, $K_L$ (L/mg) is a Langmuir constant, $K_F$ (mg/L) is a Freundlich constant, $B_1 = RT/b$, $T$ is the absolute temperature in Kelvin, $R$ is the universal gas constant (8.314 J K$^{-1}$ mol$^{-1}$), $K_T$ is the equilibrium binding constant, and the constant $B_1$ is related to the heat of adsorption.

The parameters of the different adsorption isothermal model with removing phenol and Cr(VI) are shown in Table 4. As can be seen from the correlation coefficient ($R^2$), this adsorption and degradation process is a typical monolayer adsorption [49]. $q_m$ values were, respectively, 26.61 and 60.75 mg/g for the phenol and Cr(VI) when temperature was 318 K. The adsorption capacity increases with the temperature increase, indicating that the adsorption process is endothermic, and the higher the temperature, the better the adsorption process.

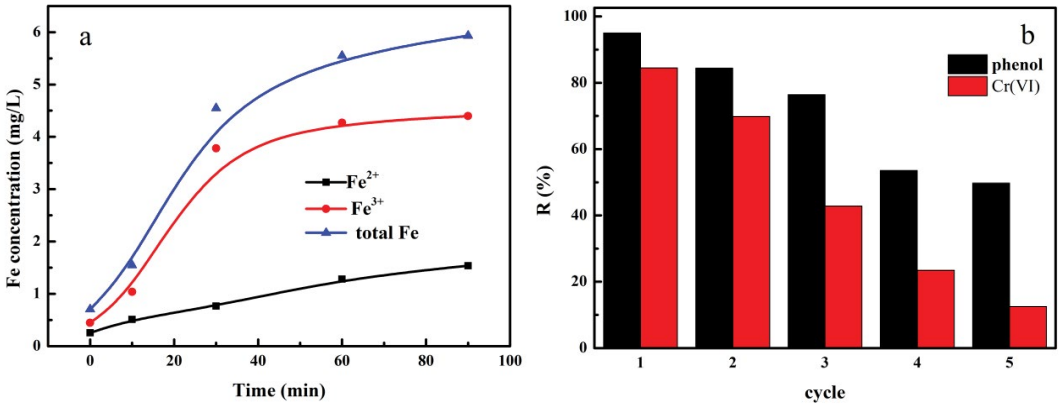


Fig. 10. Fe content in the solution after removal of pollutants (a); and reuse performance of nZVI/APT on the removal of phenol and Cr(VI) (b).

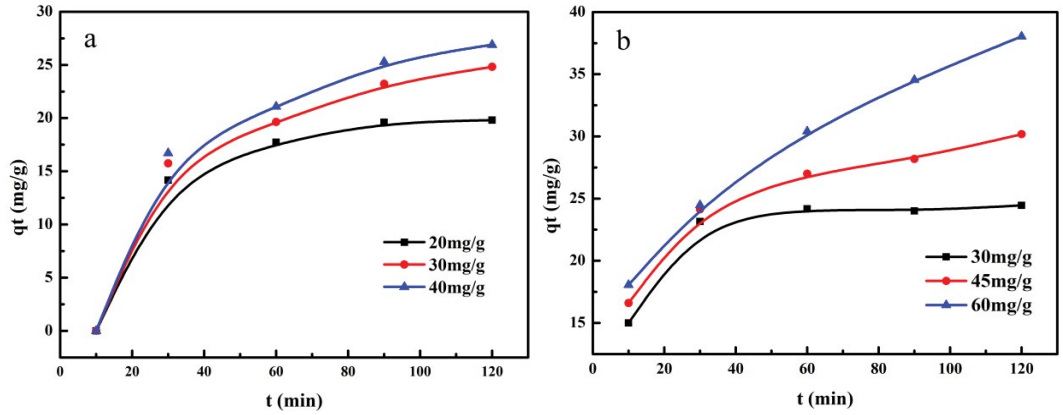


Fig. 11. Effect of contact time on removal of phenol and Cr(VI) in binary systems.

Table 3
Adsorption kinetic parameters of binary contaminant solutions

| | | Phenol adsorption $C_0$ (mg/L) | | | Cr(VI) adsorption $C_0$ (mg/L) | | |
|---|---|---|---|---|---|---|---|
| Model | Parameters | 20 | 30 | 40 | 30 | 45 | 60 |
| PFO | $K_1$ | 0.0676 | 0.0362 | 0.0215 | 0.0419 | 0.0233 | 0.0216 |
| | $q_e$ | 2.54 | 15.63 | 15.22 | 8.11 | 14.42 | 25.71 |
| | $R^2$ | 0.9752 | 0.9777 | 0.9935 | 0.8093 | 0.9379 | 0.9908 |
| PSO | $K_2$ | 0.0115 | 0.0021 | 0.0026 | 0.0102 | 0.0 030 | 0.0012 |
| | $q_e$ | 20.64 | 32.09 | 31.42 | 22.54 | 32.23 | 42.84 |
| | $R^2$ | 0.9996 | 0.9996 | 0.9932 | 0.9981 | 0.9977 | 0.9847 |
| ID | $K_p$ | 0.7089 | 1.2681 | 1.5842 | 1.0604 | 1.6262 | 2.5616 |
| | $C$ | 13.00 | 12.41 | 12.16 | 14.35 | 13.24 | 10.23 |
| | $R^2$ | 0.7712 | 0.9478 | 0.9835 | 0.5609 | 0.8871 | 0.9985 |

### 3.5. Discussion of reaction mechanism

Fig. 12 illustrates the UV-Vis spectra of Cr(VI) and phenol at different reaction times. At the beginning, the characteristic absorbance band of Cr(VI) was 540 nm before reaction, which decreased rapidly and basically disappeared in 120 min. It indicated that Cr(VI) can be reduced to Cr(III) by redox reaction with nZVI via Eq. (1) [13,50]. Fig. 11b shows that the characteristic absorbance band of phenol was at 510 nm before reaction, which decreases significantly with the progress of the reaction, it implied that phenol was oxidized and degraded by $SO_4^{\bullet-}$ radicals.

In the experiment, the removal of phenol was mainly caused by the oxidation of sulfate radicals and hydroxyl radicals. In order to determine the role of free radicals

Table 4
Adsorption isotherm parameters of binary pollution solutions

| Model | Parameters | Temperature (K)-phenol | | | Temperature (K)-Cr(VI) | | |
|---|---|---|---|---|---|---|---|
| | | 298 | 308 | 318 | 298 | 308 | 318 |
| Langmuir | $q_m$ | 23.45 | 22.19 | 26.61 | 35.50 | 34.19 | 60.75 |
| | $K_L$ | 2,643 | 28,013 | 2,278 | 2.16 | 1.35 | 122.9 |
| | $R^2$ | 0.9950 | 0.9992 | 0.9934 | 0.9980 | 0.9895 | 0.9965 |
| Freundlich | $K_F$ | 23.66 | 26.16 | 51.37 | 29.39 | 28.34 | 73.69 |
| | $1/n$ | 0.0149 | 0.0460 | 0.1536 | 0.0538 | 0.0448 | 0.1524 |
| | $R^2$ | 0.4684 | 0.9297 | 0.9715 | 0.9430 | 0.5983 | 0.8424 |
| Temkin | $B_1$ | 0.3185 | 0.9393 | 3.653 | 1.72 | 1.40 | 6.70 |
| | $K_T$ | 23.57 | 25.50 | 42.17 | $6.5 \times 10^{12}$ | $1.8 \times 10^{12}$ | $3.4 \times 10^{29}$ |
| | $R^2$ | 0.4381 | 0.9207 | 0.9801 | 0.9384 | 0.5675 | 0.8991 |

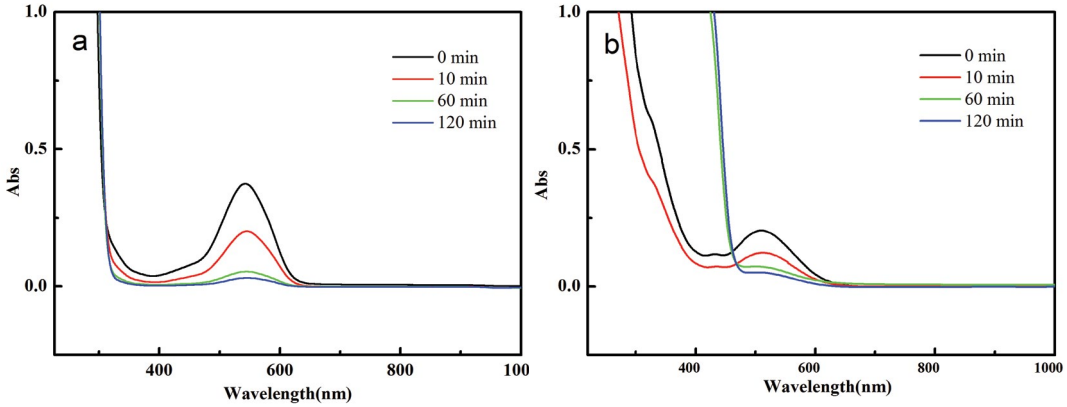


Fig. 12. UV-Visible spectral of Cr(VI) (a), phenol (b) at different reaction times and Fe content in the solution after removal of Cr(VI) and phenol (c).

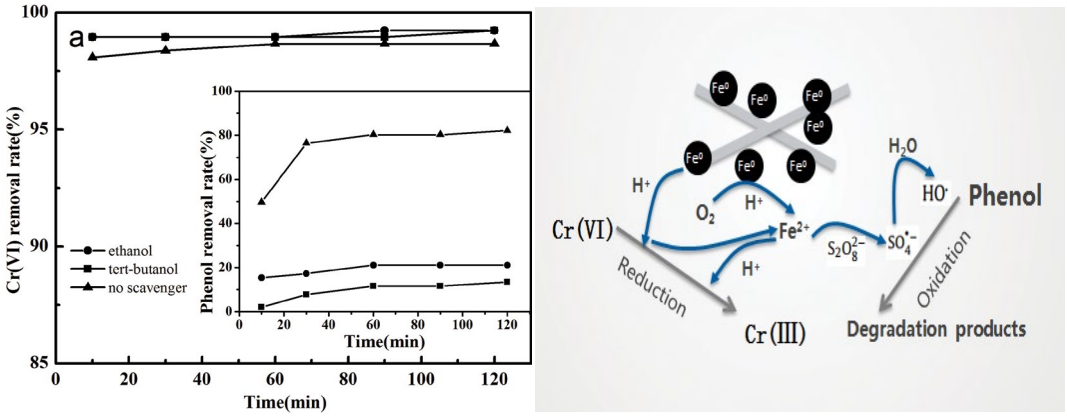


Fig. 13. Effect of radical scavengers on the Cr(VI) and phenol removal (a) and reaction mechanism (b).

in the removal of phenol, tert-butanol and ethanol were used as scavengers for sulfate radicals and hydroxyl radicals, respectively. The kinetic rate constants of tert-butyl alcohol with sulfate radicals and hydroxyl radicals were $K_{\text{TBA-hydroxylradical}} = (3.8–7.6) \times 10^8\ M^{-1}\ s^{-1}$ and $K_{\text{TBA-sulfateradical}} = (4.0–9.1) \times 10^5\ M^{-1}\ s^{-1}$ [51,52]. Ethanol was the scavenger agent of hydroxyl radicals, and its kinetic rate constant was ($K_{\text{ethanol-hydroxylradical}} = (1.2–2.8) \times 10^9\ M^{-1}\ s^{-1}$) [53]. It can be observed in the Fig. 13a that the removal efficiency of phenol drops sharply when added the scavenger, among which the phenol removal efficiency was 21.1% when ethanol was added, and the phenol removal efficiency was 13.5% in the

presence of tert-butanol. The results showed that the sulfate radicals played a major role in the removal of phenol, and the hydroxyl radical was also produced. The scavenger agent has no effect on the removal of Cr(VI), and it is confirmed that the removal of Cr(VI) was mainly the reduction of nZVI.

The reaction mechanism of the simultaneous removal of Cr(VI) and phenol by nZVI/APT combined with persulfate system as shown in Fig. 13b. At first, Cr(VI) was reduced into Cr(III) by nZVI can be described in Eq. (1). Meanwhile, the reaction process can generate $Fe^{2+}$, which can react with persulfate to produce $SO_4^{\bullet-}$ via Eq. (3).

$$5Fe^0 + Cr_2O_7^{2-} + 14H^+ \rightarrow 2Cr^{3+} + 2Fe^{2+} + 3Fe^{2+} + 3Fe^{3+} + 7H_2O \quad (11)$$

In addition, the aqueous $Fe^{2+}$ was more easily released into solution from the nZVI/APT at acidic conditions via Eq. (2). At the same time, $SO_4^{\bullet-}$ can react with $H_2O$ to produce $HO^{\bullet}$ via Eq. (4).

$$2Fe^0 + O_2 + 4H^+ \rightarrow 2Fe^2 + 2H_2O \quad (12)$$

$$Fe^{2+} + S_2O_8^{2-} \rightarrow Fe^{3+} + SO_4^{\bullet-} + SO_4^{2-} \quad (13)$$

$$SO_4^{\bullet-} + H_2O \rightarrow HO^{\bullet} + HSO_4^- \quad (14)$$

$$SO_4^{\bullet-} / HO^{\bullet} + \text{Phenol} \rightarrow \text{degradation products} \quad (15)$$

## 4. Conclusions

In this study, the nZVI/APT composite was prepared by the effective supporting of nZVI nanoparticles onto the APT rod-like structures and could be efficiently applied for simultaneous removal of Cr(VI) and phenol from aqueous solutions in the presence of persulfate. The results indicated that nZVI/APT combined persulfate system had a good synergistic effect on the simultaneous removal of Cr(VI) and phenol. APT could disperse the nZVI granules effectively, and prevent its agglomeration to enhance reactivity of nZVI. The Cr(VI) removal was mainly due to the reduction of nZVI, while the degradation of phenol mainly contributes to the $SO_4^{\bullet-}$ from the decomposition of persulfate. Persulfate can produce more oxidative sulfate radical anions with $Fe^{2+}$ and improve its reactivity. Under pH = 3 acidic condition, the batch experiments confirmed that Cr(VI) and phenol removal efficiencies after 60 min were about 98.7% and 80.3%, respectively. The study showed that nZVI/APT combined persulfate system has a great potential as an efficient adsorbent for water containing pollutants such as heavy metals and organic compounds.

## Acknowledgments

This work was supported by the National Natural Science Foundation of China (NSFC; 51763015, 51503092), the Foundation for Innovation Groups of Basic Research in Gansu Province (No. 1606RJIA322), the Program for Hongliu First-class Discipline Construction in Lanzhou University of Technology.

## References

[1] L.N. Shi, X. Zhang, Z.L. Chen, Removal of chromium (VI) from wastewater using bentonite-supported nanoscale zero-valent iron, Water Res., 45 (2011) 886–892.
[2] W. Li, Y.K. Tang, Y.T. Zeng, Z.F. Tong, D.W. Liang, W.W. Cui, Adsorption behavior of Cr(VI) ions on tannin-immobilized activated clay, Chem. Eng. J., 193–194 (2012) 88–95.
[3] M. Gheju, I. Balcu, Removal of chromium from Cr(VI) polluted wastewaters by reduction with scrap iron and subsequent precipitation of resulted cations, J. Hazard. Mater.,196 (2011) 131–138.
[4] H. Sarahney, X.H. Mao, A.N. Alshawabkeh, The role of iron anode oxidation on transformation of chromium by electrolysis, Electrochim. Acta, 86 (2012) 96–101.
[5] A. Kumar, C. Guo, G. Sharma, D. Pathania, M. Naushad, S. Kalia, Magnetically recoverable $ZrO_2/Fe_3O_4$/chitosan nanomaterials for enhanced sunlight driven photoreduction of carcinogenic Cr(VI) and dechlorination and mineralization of 4-chlorophenol from simulated waste water, RSC Adv., 6 (2016) 13251–13263.
[6] Y.T. Lin, C.J. Liang, J.H. Chen, Feasibility study of ultraviolet activated persulfate oxidation of phenol, Chemosphere, 82 (2011) 1168–1172.
[7] R. Vinu, M. Giridhar, Kinetics of simultaneous photocatalytic degradation of phenolic compounds and reduction of metal ions with nano-$TiO_2$, Environ. Sci. Technol., 42 (2008) 913–919.
[8] R.L. Qiu, D.D. Zhang, Z.H. Diao, X.F. Huang, C. He, J.L. Morel, Y. Xiong, Visible light induced photocatalytic reduction of Cr(VI) over polymer-sensitized $TiO_2$ and its synergism with phenol oxidation, Water Res., 46 (2012) 2299–2306.
[9] R.X. Mu, Z.Y. Xu, L.Y. Li, Y. Shao, H.Q. Wan, S.R. Zheng, On the photocatalytic properties of elongated $TiO_2$ nanoparticles for phenol degradation and Cr(VI) reduction, J. Hazard. Mater., 176 (2010) 495–502.
[10] C.X. Zhang, Y.B. Sun, Z.Q. Yu, G.Y. Zhang, J.W. Feng, Simultaneous removal of Cr(VI) and acid orange 7 from water solution by dielectric barrier discharge plasma, Chemosphere, 191 (2018) 527–536.
[11] M. Naushad, Surfactant assisted nano-composite cation exchanger: Development, characterization and applications for the removal of toxic $Pb^{2+}$ from aqueous medium, Chem. Eng. J., 235 (2014) 100–108.
[12] A.A. Alqadami, Mu. Naushad, Z.A. Alothman, A.A. Ghfar, Novel metal-organic framework (MOF) based composite material for the sequestration of U(VI) and Th(IV) metal ions from aqueous environment, ACS Appl. Mater. Interface, 41 (2017) 36026–36037.
[13] X.C. Yin, W. Liu, J.R. Ni, Removal of coexisting Cr(VI) and 4-chlorophenol through reduction and Fenton reaction in a single system, Chem. Eng. J., 248 (2014) 89–97.
[14] X. He, H.M. Yang, Au nanoparticles assembled on palygorskite: Enhanced catalytic property and $Au–Au_2O_3$ coexistence, J. Mol. Catal. A, 379 (2013) 219–224.
[15] L.S. Krishna, K. Soontarapa, A. Yuzir, V.A. Kumar, W.Y.W. Zuhairi, Kaolin-nano scale zero-valent iron composite(K-nZVI): synthesis, characterization and application for heavy metal removal, Desal. Wat. Treat., 100 (2017) 168–177.
[16] H. Xu, W.G. Tian, Y.J. Zhang, J. Tang, Z.T. Zhao, Y. Chen, Reduced graphene oxide/attapulgite-supported nanoscale zero-valent iron removal of Acid Red 18 from aqueous solution, Water Air Soil Pollut., 229 (2018) 1–16.
[17] H.J. Zhu, Y.F. Jia, X. Wu, H. Wang, Removal of arsenic from water by supported nano zero-valent iron on activated carbon, J. Hazard. Mater., 172 (2009) 1591–1596.
[18] B. Mu, A.Q. Wang, Adsorption of dyes onto palygorskite and its composites: A review, J. Environ. Chem. Eng., 4 (2016) 1274–1294.

[19] R.L. Frost, Y.F. Xi, H.P. He, Synthesis, characterization of palygorskite supported zero-valent iron and its application for methylene blue adsorption, J. Colloid Interface Sci., 341 (2010) 153–161.
[20] J.C. Yan, M. Lei, L.H. Zhu, M.N. Anjum, J. Zou, H.Q. Tang, Degradation of sulfamonomethoxine with $Fe_3O_4$ magnetic nanoparticles as heterogeneous activator of persulfate, J. Hazard. Mater., 186 (2011) 1398–1404.
[21] X.L. Zou, T. Zhou, J. Mao, X.H. Wu, Synergistic degradation of antibiotic sulfadiazine in a heterogeneous ultrasound-enhanced $Fe^0$/persulfate Fenton-like system, Chem. Eng. J., 257 (2014) 36–44.
[22] H. Hori, A. Yamamoto, E. Hayakawa, S. Taniyasu, N. Yamashita, S. Kutsuna, H. Kiatagawa, R. Arakawa, Efficient decomposition of environmentally persistent perfluorocarboxylic acids by use of persulfate as a photochemical oxidant, Environ. Sci. Technol., 39 (2005) 2383–2388.
[23] A. Romero, A. Santos, F. Vicente, C. González, Diuron abatement using activated persulphate: effect of pH, Fe(II) and oxidant dosage, Chem. Eng. J., 162 (2010) 257–265.
[24] H.R. Dong, Q. He, G.M. Zeng, L. Tang, L.H. Zhang, Y.K. Xie, Y.L Zeng, F. Zhao, Degradation of trichloroethene by nanoscale zero-valent iron (nZVI) and nZVI activated persulfate in the absence and presence of EDTA, Chem. Eng. J., 316 (2017) 410–418.
[25] H.X. Li, J.Q. Wan, Y.W. Ma, Y. Wang, M.Z. Huang, Influence of particle size of zero-valent iron and dissolved silica on the reactivity of activated persulfate for degradation of acid orange 7, Chem. Eng. J., 237 (2014) 487–496.
[26] S.H. Do, Y.J. Kwon, S.H. Kong, Effect of metal oxides on the reactivity of persulfate/Fe(II) in the remediation of diesel-contaminated soil and sand, J. Hazard. Mater., 182 (2010) 933–936.
[27] J.Y. Zhao, Y.B. Zhang, X. Quan, S. Chen, Enhanced oxidation of 4-chlorophenol using sulfate radicals generated from zero-valent iron and peroxydisulfate at ambient temperature, Sep. Purif. Technol., 71 (2010) 302–307.
[28] Z.H. Diao, X.R. Xu, D. Jiang, L.J. Kong, Y.X. Sun, Y.X. Hu, Q.W. Hao, H. Chen, Bentonite-supported nanoscale zero-valent iron/persulfate system for the simultaneous removal of Cr(VI) and phenol from aqueous solutions, Chem. Eng. J., 302 (2016) 213–222.
[29] Y. Yin, M. Zeng, J. Liu, W. Tang, H. Dong, R. Xia, R. Yu, Enhanced high-frequency absorption of anisotropic $Fe_3O_4$/graphene nanocomposites, Sci. Rep., 6 (2016) 25075.
[30] Q.L. Ma, W.S. Yu, X.T. Dong, J.X. Wang, G.X. Liu, Janus nanobelts: fabrication, structure and enhanced magnetic-fluorescent bifunctional performance, Nanoscale, 6 (2014) 2945–2952.
[31] B. Mu, A.Q. Wang, One-pot fabrication of multifunctional superparamagnetic attapulgite/$Fe_3O_4$/polyaniline nanocomposites served as an adsorbent and catalyst support, J. Mater. Chem. A, 3 (2015) 281–289.
[32] Y. Chen, Z.H. Lin, R.R. Hao, H. Xu, Chengyu Huang Rapid adsorption and reductive degradation of Naphthol Green B from aqueous solution by polypyrrole/attapulgite composites supported nanoscale zero-valent iron, J. Hazard. Mater., 371 (2019) 8–17.
[33] Mu. Naushad, T. Ahamad, B.M. Al-Maswari, A.A. Alqadami, S.M. Alshehri, Nickel ferrite bearing nitrogen-doped mesoporous carbon as efficient adsorbent for the removal of highly toxic metal ion from aqueous medium, Chem. Eng. J., 330 (2017) 1351–1360.
[34] Z.F. Ren, X. Xu, X. Wang, B.Y. Gao, Q.Y. Yue, W. Song, L. Zhang, H.T. Wang, FTIR, Raman, and XPS analysis during phosphate, nitrate and Cr(VI) removal by amine cross-linking biosorbent, J. Colloid Interface Sci., 468 (2016) 313–323.
[35] S.H. Zhang, M.F. Wu, T.T. Tang, Q.J. Xing, C.Q. Peng, F. Li, H. Liu, X.B. Luo, J.P. Zou, X.B. Min, J.M. Luo, Mechanism investigation of anoxic Cr(VI) removal by nano zero-valent iron based on XPS analysis in time scale, Chem. Eng. J., 335 (2018) 945–953.
[36] X. Liu, X. Xu, J. Sun, A. Alsaedi, T. Hayat, J. Li, X. Wang, Insight into the impact of interaction between attapulgite and graphene oxide on the adsorption of U(VI), Chem. Eng. J., 343 (2018) 217–224.
[37] B. Rhouta, E. Zatile, L. Bouna, O. Lakbita, F. Maury, L. Daoudi, M.C. Lafont, M.B. Amjoud, F. Senocq, A. Jada, Comprehensive physicochemical study of dioctahedral palygorskite-rich clay from Marrakech High Atlas (Morocco), Phys. Chem. Miner., 40 (2013) 411–424.
[38] H. Kusic, I. Peternel, N. Koprivanac, A. Loncaric Bozic, Iron-activated persulfate oxidation of an azo dye in model wastewater: influence of iron activator type on process optimization, J. Environ. Eng., 137 (2011) 454–463.
[39] O.M. Ontanon, C. Landi, A. Carleo, A. Gagliardi, L. Bianchi, P.S. Gonzalez, E. Agostini, L. Bini, What makes A. guillouiae SFC 500-1A able to co-metabolize phenol and Cr(VI)? A proteomic approach, J. Hazard. Mater., 354 (2018) 215–224.
[40] C. Dong, J. Ji, B. Shen, M. Xing, J. Zhang, Enhancement of $H_2O_2$ decomposition by the Co-catalytic effect of WS2 on the Fenton reaction for the synchronous reduction of Cr(VI) and remediation of phenol, Environ. Sci. Technol., 52 (2018) 11297–11308.
[41] A. Chen, Z. Bian, J. Xu, X. Xin, H. Wang, Simultaneous removal of Cr(VI) and phenol contaminants using Z-scheme bismuth oxyiodide/reduced graphene oxide/bismuth sulfide system under visible-light irradiation, Chemosphere, 188 (2017) 659–666.
[42] S.M. Alshehri, Mu. Naushad, T. Ahamad, Z.A. ALOthman, A. Aldalbahi, Synthesis, characterization of curcumin based ecofriendly antimicrobial bio-adsorbent for the removal of phenol from aqueous medium, Chem. Eng. J., 254 (2014) 181–189.
[43] Z.A. Al-Othman, R. Ali, M. Naushad, Hexavalent chromium removal from aqueous medium by activated carbon prepared from peanut shell: adsorption kinetics, equilibrium and thermodynamic studies, Chem. Eng. J., 184 (2012) 238–247.
[44] A. Zeid, ALOthman, Mu. Naushad, A. Rahmat, Kinetic, equilibrium isotherm and thermodynamic studies of Cr(VI) adsorption onto low-cost adsorbent developed from peanut shell activated with phosphoric acid, Environ. Sci. Pollut. Res., 20 (2013) 3351–3365.
[45] X.Y. Wei, N.Y. Gao, C.J. Li, Y. Deng, S.Q. Zhou, L. Li, Zero-valent iron (ZVI) activation of persulfate (PS) for oxidation of bentazon in water, Chem. Eng. J., 285 (2016) 660–670.
[46] C.J Liang, I.L. Lee, I.Y. Hsu, C.P. Liang, Y.L. Lin, Persulfate oxidation of trichloroethylene with and without iron activation in porous media, Chemosphere, 70 (2008) 426–435.
[47] A. Maria Leah Flor. De Castro, Melody Love B. Abad, Divine Angela G. Sumalinog, Ralf Ruffel M. Abarca, Peerasak Paoprasert, Mark Daniel G. de Luna, Adsorption of Methylene Blue dye and Cu(II) ions on EDTA-modifiedbentonite: Isotherm, kinetic and thermodynamic studies, J. Environ. Chem. Eng., 6 (2018) 2803–2811.
[48] Y. Chen, W.C. Long, H. Xu, Efficient removal of Acid Red 18 from aqueous solution by in-situ polymerization of polypyrrole-chitosan composites, J. Mol. Liq., 287 (2019) 110888.
[49] M. Zhang, Q. Yao, C. Lu, Z. Li, W. Wang, Layered double hydroxide-carbon dot composite: high-performance adsorbent for removal of anionic organic dye, ACS Appl. Mater. Interface, 6 (2014) 20225–20233.
[50] D. Lv, J.S. Zhou, Z. Cao, J. Xu, Y.L. Liu, Y.Z. Li, K.L. Yang, Z.M. Lou, L.P. Lou, X.H. Xu, Mechanism and influence factors of chromium(VI) removal by sulfidemodified nanoscale zerovalent iron, Chemosphere, 224 (2019) 306–315.
[51] G.P. Anipsitakis, D.D. Dionysiou, Radical generation by the interaction of transition metals with common oxidants, Environ. Sci. Technol., 38 (2004) 3705.
[52] Y.F. Ji, C. Ferronato, A. Salvador, X. Yang, J.M. Chovelon, Degradation of ciprofloxacin and sulfamethoxazole by ferrous-activated persulfate: implications for remediation of groundwater contaminated by antibiotics, Sci. Total Environ., 472 (2014) 800–808.
[53] A.L. Teel, R.J. Watts, Degradation of carbon tetrachloride by modified Fenton's reagent, J. Hazard. Mater., 94 (2002) 179–189.